

RESEARCH

Open Access



# Post-exposure intranasal IFN $\alpha$ suppresses replication and neuroinvasion of Venezuelan Equine Encephalitis virus within olfactory sensory neurons

Matthew D. Cain<sup>1,2</sup>, N. Rubin Klein<sup>2</sup>, Xiaoping Jiang<sup>1,2</sup>, Hamid Salimi<sup>1,2</sup>, Qingping Wu<sup>1,2</sup>, Mark J. Miller<sup>2</sup>, William B. Klimstra<sup>5</sup> and Robyn S. Klein<sup>1,2,3,4\*</sup>

## Abstract

**Background** Venezuelan Equine Encephalitis virus (VEEV) may enter the central nervous system (CNS) within olfactory sensory neurons (OSN) that originate in the nasal cavity after intranasal exposure. While it is known that VEEV has evolved several mechanisms to inhibit type I interferon (IFN) signaling within infected cells, whether this inhibits virologic control during neuroinvasion along OSN has not been studied.

**Methods** We utilized an established murine model of intranasal infection with VEEV and a repository of scRNAseq data from IFN-treated OSN to assess the cellular targets and IFN signaling responses after VEEV exposure.

**Results** We found that immature OSN, which express higher levels of the VEEV receptor LDLRAD3 than mature OSN, are the first cells infected by VEEV. Despite rapid VEEV neuroinvasion after intranasal exposure, olfactory neuroepithelium (ONE) and olfactory bulb (OB) IFN responses, as assessed by evaluation of expression of interferon signaling genes (ISG), are delayed for up to 48 h during VEEV neuroinvasion, representing a potential therapeutic window. Indeed, a single intranasal dose of recombinant IFN $\alpha$  triggers early ISG expression in both the nasal cavity and OB. When administered at the time of or early after infection, IFN $\alpha$  treatment delayed onset of sequelae associated with encephalitis and extended survival by several days. VEEV replication after IFN treatment was also transiently suppressed in the ONE, which inhibited subsequent invasion into the CNS.

**Conclusions** Our results demonstrate a critical and promising first evaluation of intranasal IFN $\alpha$  for the treatment of human encephalitic alphavirus exposures.

\*Correspondence:

Robyn S. Klein  
rklein@wustl.edu

<sup>1</sup> Center for Neuroimmunology & Neuroinfectious Diseases, Washington University School of Medicine, St. Louis, MO, USA

<sup>2</sup> Departments of Medicine, Washington University School of Medicine, St. Louis, MO, USA

<sup>3</sup> Departments of Pathology and Immunology, Washington University School of Medicine, St. Louis, MO, USA

<sup>4</sup> Departments of Neurosciences, Washington University School of Medicine, St. Louis, MO, USA

<sup>5</sup> Department of Immunology and Center for Vaccine Research, University of Pittsburgh, Pittsburgh, PA, USA

## Introduction

Alphaviruses are members of the *Togaviridae* family of enveloped single-strand RNA arboviruses transmitted by mosquitoes. The arthritogenic Old World alphaviruses include Chikungunya virus (CHIKV), Sindbis virus (SINV), Semliki Forest virus (SFV) and Ross River virus (RRV). The New World alphaviruses, including Venezuelan, Eastern, and Western equine encephalitis viruses (VEEV, EEEV, WEEV), are characterized by the ability to infect the central nervous system (CNS) leading



© The Author(s) 2024. **Open Access** This article is licensed under a Creative Commons Attribution 4.0 International License, which permits use, sharing, adaptation, distribution and reproduction in any medium or format, as long as you give appropriate credit to the original author(s) and the source, provide a link to the Creative Commons licence, and indicate if changes were made. The images or other third party material in this article are included in the article's Creative Commons licence, unless indicated otherwise in a credit line to the material. If material is not included in the article's Creative Commons licence and your intended use is not permitted by statutory regulation or exceeds the permitted use, you will need to obtain permission directly from the copyright holder. To view a copy of this licence, visit <http://creativecommons.org/licenses/by/4.0/>. The Creative Commons Public Domain Dedication waiver (<http://creativecommons.org/publicdomain/zero/1.0/>) applies to the data made available in this article, unless otherwise stated in a credit line to the data.

to meningitis and encephalitis, with acute and chronic neurological sequelae [1]. VEEV–IAB/IC serotypes are linked to human and equine epizootic outbreaks, while VEEV–enzootic cycles occur between rodents and mosquitoes. In addition to natural routes of infection, VEEV, along with EEEV and WEEV, may enter the CNS after intranasal (i.n.) exposure, highlighting the possibility of VEEV weaponization via aerosolization. As there are no approved vaccines for public distribution and no treatments for CNS infection with VEEV, there is a need to understand viral entry and innate immune responses along these routes to develop protective measures.

Studies of murine infections with VEEV–enzootic subtype ZPC-738 show that VEEV can enter the CNS through hematogenous spread across an intact blood–brain barrier (BBB) and via anterograde transport along cranial nerves [2, 3]. Astrocytes are the first infected cell during hematogenous entry, with further dissemination within the CNS via infected neurons [3]. Intranasal (i.n.) exposure leads to infection of the olfactory sensory neurons (OSN) of the nasal cavity neuroepithelium, leading to neuroinvasion along axons that cross the cribriform plate into the olfactory bulbs (OB), which results in widespread CNS infection and lethality. Low Density Lipoprotein Receptor Class A Domain Containing 3 (LDLRAD3), was identified as a receptor for VEEV [4–6]. Global deletion of LDLRAD3 suppresses systemic infection during the peripheral prodrome phase during which peripheral mononuclear cells become infected [4]. While prophylactic administration of LDLRAD3–Fc fusion proteins suppresses peripheral infection and neuroinvasion, this does not suppress all replication within the brain. It is not known whether LDLRAD3 is expressed by neurons within the olfactory routes of invasion.

Type I interferons (IFN) signal via auto- and paracrine activation of JAK/STAT downstream of the IFN receptor (IFNAR), which is necessary to control initial VEEV infection [7]. However, VEEV has evolved several mechanisms to inhibit IFNAR signaling within infected cells, including host transcription and translation shut-off by VEEV capsid and non-structural protein (nsP)2, and nsP inhibition of IFNAR-induced STAT1 activation via mechanisms independent of host shut off [8–12]. While systemic, pre-exposure (> 24 h) administration of exogenous IFN controls aerosolized virulent VEEV infection and enhances survival in mice [13], no studies have examined whether IFN has benefit post-exposure. Overall, the multiple routes of entry into the CNS may require specific treatment strategies that depend on the site of initial infection. Alternative to systemic IFN administration, intranasal IFN treatment may uniquely protect the CNS during aerosolized infection. Intranasally administered IFN $\beta$  distributes throughout the CNS along

olfactory tracts in rats and non-human primates [14, 15]. This route of administration resulted in higher concentrations of the cytokine in the brain, suggesting that high doses of IFN may additionally protect susceptible neurons distant from initial sites of neuroinvasion. Intranasal administration of IFN $\alpha$  is well-tolerated, making this strategy potentially viable for post-exposure treatment of aerosolized VEEV infection [16].

In this study we demonstrate that VEEV initially targets GAP43+ immature (i)OSN within the olfactory neuroepithelium (ONE). Tropism toward iOSNs correlated with higher LDLRAD3 expression within iOSN versus mature (m)OSN, but no broad deficits in innate immunity, as assessed via scRNAseq, were observed in iOSN that would contribute to their enhanced infectivity over mOSN. Despite rapid VEEV neuroinvasion, host nasal cavity and CNS IFN responses are delayed for up to 48 h during VEEV neuroinvasion, representing a potential therapeutic window. Thus, we evaluated the efficacy of single dose recombinant IFN $\alpha$  administered intranasally at the time of or early after infection (0–3 h post-infection), which was able to trigger ISG expression in both the nasal cavity and OB. IFN $\alpha$  treatment delayed onset of sequelae associated with encephalitis and extended survival by several days. VEEV replication after IFN treatment was also transiently suppressed in the ONE, which inhibited subsequent invasion into the CNS. Together these data identify iOSN that express high levels of LDLRAD3 as the initial target of VEEV, define OSN ISG transcriptomic signatures, and demonstrate the efficacy of intranasal delivery of IFN $\alpha$  to protect sites critical to early VEEV–CNS infection. Our results demonstrate a critical and promising first evaluation of such a treatment strategy for human encephalitic alphavirus infection.

## Materials and methods

### Animals

C57BL/6J mice were purchased from Jackson Laboratories (Bar Harbor, ME). Animals were housed under pathogen-free conditions in Washington University School of Medicine animal facilities. All experiments were performed in compliance with Washington University animal studies guidelines.

### Mouse model of VEEV encephalitis

8–10-week-old male mice were inoculated intranasally (10  $\mu$ L per nostril) with VEEV strain ZPC-738 or ZPC-738–eGFP (10 or 50 pfu, respectively) under anesthesia. ZPC-738–eGFP was a generous gift of William Klimstra (Pittsburg, PA). ZPC-738–eGFP was generated by subgenomic insertion of GFP as a cleavable element between the capsid and PE2 structural proteins, described previously [17]. Parental ZPC-738 or ZPC-738–eGFP are

uniformly lethal at 10 pfu. GFP genomic VEEV modification exhibited slight attenuation, delayed expansion/neuroinvasion during early infection (unpublished data), and extended MST [17]. To account for this, ZPC-738-eGFP studies were performed at 50 pfu. Mice were monitored daily for weight loss and scored daily for encephalitic sequelae. Moribund mice were sacrificed by CO<sub>2</sub> asphyxiation and recorded as dead the following day. Encephalitic score represents a progressive range of behaviors: (1) hunched, ruffled fur, (2) altered gait, slow movement, (3) not moving but responsive, (4) not moving, poorly responsive but upright, (5) moribund, (6) dead.

#### Perfusion–fixation and immunohistochemistry

At various times post-infection, mice were anesthetized followed by extensive cardiac perfusion with PBS and perfusion fixation with 4% paraformaldehyde (PFA) in PBS. Tissue was immersion-fixed for an additional 24 h in 4% PFA. For slice preparations of mouse nasal cavities, skulls were decalcified by multiple exchanges 0.5 M EDTA (pH 7.4) in PBS over 7 days followed by PBS and cryoprotection (two-exchanges of 30% sucrose for at least 48 h) and embedding in OCT (Fisher). 10 µm-thick fixed-frozen sagittal sections were hydrated with PBS and blocked for 1 h in blocking solution, 5% normal donkey serum (Santa Cruz Biotechnology) with 0.1% Triton X-100 (Sigma-Aldrich). After block, slides were exposed to primary antibody at 4 °C overnight, washed with PBS and incubated with Alexa Fluor donkey secondary antibodies (Invitrogen) for 1 h at room temperature. Antibodies used: chicken anti-GFP (Abcam, 13970), goat anti-OMP (Wako Chemicals, 544-10001), rabbit anti-GAP43 (Novus Biologicals, NB300-143). Images were acquired using a Zeiss LSM 880 confocal laser scanning microscope and processed using Zen3.3 (Zeiss) and Image J. Quantification of immunofluorescence was performed using ImageJ.

#### In situ hybridization

In situ hybridization staining of decalcified sagittal skull section (described above) were performed using Advanced Cell Diagnostics (ACD) RNAscope system and probes. After rehydration of slides in PBS, slides were baked (30 min at 60 °C) and post-fixed in 4% PFA. Slides were dehydrated in progressive ethanol washes (50%, 70%, 100%, 100%, 5 min), air dried, treated with hydrogen peroxide (10 min). For in situ hybridization alone, Advanced Cell Diagnostics RNAscope 2.5 HD Detection Reagent—RED (322360) using standard manufactures protocol, RNAscope Target Retrieval Reagent (95–98 °C, 10 min), RNAscope Protease Plus (30 min), and standard hybridization with the Ldlrad3 probe (ACD), signal amplification, and counter-staining

with DAPI. For combined RNA–protein co-imaging, RNAscope Multiplex Fluorescent v2 Assay (323100) along with RNA–Protein Co-detection Ancillary Kit (323180) was used utilizing the Integrated Co-Detection Workflow (ICW). Following baking, post-fixation, dehydration, and hydrogen peroxide treatment, slides were immersed in Co-Detection Target Retrieval (95–98 °C, 5 min). Tissue was blocked and incubated overnight with GAP43 and OMP primary antibodies (see above) using Co-Detection Antibody Diluent. Samples were post-primary fixed using 10% neutral buffered formalin (30 min, RT) prior to RNAscope Protease Plus treatment, hybridization with the V-VEEV-ZPC-738 (ACD, 876381), Mm-Ldlrad3 (ACD, 872101), or dapB negative control probes (ACD, 310043), signal amplification with Opal 650 Dye (Akoya Biosciences, OP-001005) in RNAscope Multiplex TSA Buffer. Tissues were labeled with Alexa-conjugated secondary antibodies (see above) in Co-Detection Antibody Diluent, counter-stained with DAPI, and mounted in Prolong Gold (Invitrogen #P36930). Tissue were imaged as described above.

#### Interferon treatment of mouse nasal mucosa

scRNAseq data set of intranasal IFN $\alpha$  mice was originally generated as described previously. Briefly, 8–10-week-old C57BL6/J mice received either 200 ng of IFN $\alpha$  (Biolegend 752802,  $\sim 1 \times 10^4$  U) or saline intranasally ( $N=2$ ), Respiratory and olfactory mucosa were isolated 12 h later. Single cells suspension were generated in media containing Liberase (Roche) and DNase I (Roche) and loaded on duplicate Seq-Well S3 arrays for sequencing using Illumina NextSeq. Raw expression counts for cells previously defined within Immature Olfactory Sensory Neurons and Olfactory Sensory Neurons (saline and IFN $\alpha$  treated) clusters were downloaded from published data set. [https://singlecell.broadinstitute.org/single\\_cell/study/SCP832?scpr=the-alexandria-project#study-summary](https://singlecell.broadinstitute.org/single_cell/study/SCP832?scpr=the-alexandria-project#study-summary). Data were normalized and scaled using the Seurat R package (<https://satijalab.org/seurat/>). Differential expression tests between mature and immature OSNs within saline-treated group or between saline-treated or IFN $\alpha$ -treated OSNs were performed using Seurat FindAllMarkers function with default settings and Wilcoxon rank sum test ( $P$  value threshold=0.05). GSEA analysis was performed using fgsea function from (fgsea, using the murine Gene Ontology gene sets (MSigDB). Genes were ordered by the Log<sub>2</sub> fold change using Seurat FindMarkers function. Violin plots and heatmaps were generated using Seurat R package. Volcano plots were generated using the EnhancedVolcano package.

### Administration of IFN $\alpha$

Recombinant mouse IFN $\alpha$ 1 (Biolegend, 751806) was administered intranasally. Control mice were similarly administered vehicle solution of 0.1% bovine serum albumin (BSA) in PBS. Doses ( $8 \times 10^4$  U, 10  $\mu$ L/nostril) administered at time of infection were suspended in the inoculum under brief isoflurane anesthesia. Subsequent doses ( $8 \times 10^4$  U, 5  $\mu$ L/nostril) were administered at 1–3 h post-infection (hpi), as indicated, under brief isoflurane anesthesia.

### RNA isolation and quantitative RT-PCR

CNS and nasal cavity tissue was collected isolated from cardiac-perfused mice at various timepoints after intranasal ZPC-738 (10 pfu i.n.) infection and/or IFN $\alpha$  treatment. Total nasal cavity tissue, including the nasal turbinates, was collected using forceps following removal of the nasal bone along the nasomaxillary suture. RNA was isolated from tissues using RNeasy kit (Qiagen) according to manufacturer's instructions, and quantified using a NanoDrop (Thermo Scientific). Following DNase I treatment (Invitrogen) of RNA samples (1  $\mu$ g) was reverse transcribed using Taqman Reverse Transcriptase kit (Applied Biosystems). qRT-PCR was performed using Power SYBR Green (Applied Biosystems) on a CFX384 PCR Detection System (Bio-Rad) using manufacturer's recommended cycle parameters. Values are reported as the Cq values for target genes normalized to Cq values of GAPDH ( $Cq_{\text{gene}} - Cq_{\text{GAPDH}}$ ). Primers (5'–3') used are reported in Additional file 1: Table S1.

### Virologic analysis

At various post-infection intervals, nasal cavity and CNS tissue was collected from ZPC-738-infected mice after extensive cardiac perfusion with PBS. Viral titers were determined using standard plaque assay techniques by serial dilution of tissue homogenates over BHK cells, as described previously [18].

### Statistical analyses

Reported values are mean values  $\pm$  standard error of the mean (SEM). Statistical analysis was performed using GraphPad Prism 7 software. Survival curves were

analyzed by Mantel–Cox test. Cytokine and ISG expression in infected mice were analyzed via one-way analysis of variance (ANOVA), Bonferroni's post hoc test was subsequently used for comparison of individual means. ISG expression following IFN $\alpha$  treatment were analyzed by unpaired Welch's *t* test with Welch's correction, as appropriate for samples with different variances. Weight loss and encephalitic sequelae scores were compared via two-way repeated measure ANOVA, followed by Bonferroni's post hoc test. *P* values  $P < 0.05$  were considered significant. Statistical values are indicated as follows \*,  $P < 0.05$ ; \*\*,  $P < 0.01$ ; \*\*\*,  $P < 0.001$ , \*\*\*\*,  $P < 0.0001$  unless otherwise stated.

## Results

### Immature olfactory sensory neurons are the initial site of VEEV infection after intranasal exposure

Intranasal (i.n.) infection with an enzootic strain of VEEV (ID, ZPC-738; herein VEEV) results in rapid progression of weight loss and onset of encephalitic symptoms, with a mean survival time (MST) of 6.5 dpi (Additional file 2: Fig. S1A). In previous studies we demonstrated i.n. VEEV infection rapidly disseminates into the OB and CTX within 24 h, with viral loads peaking at 2–3 dpi in the OB and at 4–6 dpi in CTX, hindbrain regions, and spinal cord, highlighting early infection to the OB as a critical period to control VEEV dissemination along the olfactory route after i.n. exposure [3]. To define cellular tropism within the ONE we utilized a reporter strain of VEEV, ZPC-738-GFP, which exhibits similar virulence as the parent strain and labels infected cells green, in conjunction with OSN markers, all detected via double-label confocal microscopy [17]. Within the infected ONE, GAP43+ iOSNs are the earliest site of infection at 1 dpi [Fig. 1A, B (top) white arrowhead]. OMP+ mOSN were also infected at this timepoint [Fig. 1A (open arrowheads)]. GFP is also detected within GAP43+ and OMP+ OSN axons traversing the cribriform plate and within the olfactory nerve layer (ONL) of the OB (Fig. 1B, bottom). VEEV–RNA, as assessed via fluorescent in situ hybridization, is also detected within GAP43+ and OMP+ axons within the ONE and OB ONL (Fig. 1C, Additional file 2: Fig. S1B). By 3 dpi, GFP+ cells

(See figure on next page.)

**Fig. 1** Neuroinvasion of intranasal VEEV involves early infection and anterograde transport from immature OSNs. **A, B** Immunostaining of murine ONE following intranasal VEEV–ZPC–GFP infection (50 pfu, 1 dpi). Solid and hollow arrowheads indicate GFP-labeling of infected GAP43+ immature OSNs (red) and OMP+ mature OSNs (blue), respectively. **B** GFP-labeling of OMP+ and GAP43+ OSN axons in the ONE and outer nerve layer of the olfactory bulb following ZPC–GFP infection (50 pfu, 1 dpi). **C** FISH staining of VEEV genome (magenta) within the OMP+ (red) and GAP43+ (green) OSN axons in the ONE and outer nerve layer of the olfactory bulb (ZPC-738, 10 pfu, 1 dpi). **D** Cartoon depiction of sagittal section nasal cavity and forebrain. ONE (cyan), OB (green), olfactory tract (dark green) are indicated. **E** Immunostaining of intranasal VEEV–ZPC–GFP infection (50 pfu, 3 dpi) of sagittal sectioned nasal cavity and forebrain, and rostral sequence of coronal slices (Bregma ~ 2.0 and – 2.0 mm) depicting VEEV–GFP dissemination along lateral olfactory tract and piriform cortex. All images depict representative infections from  $N = 3$  mice

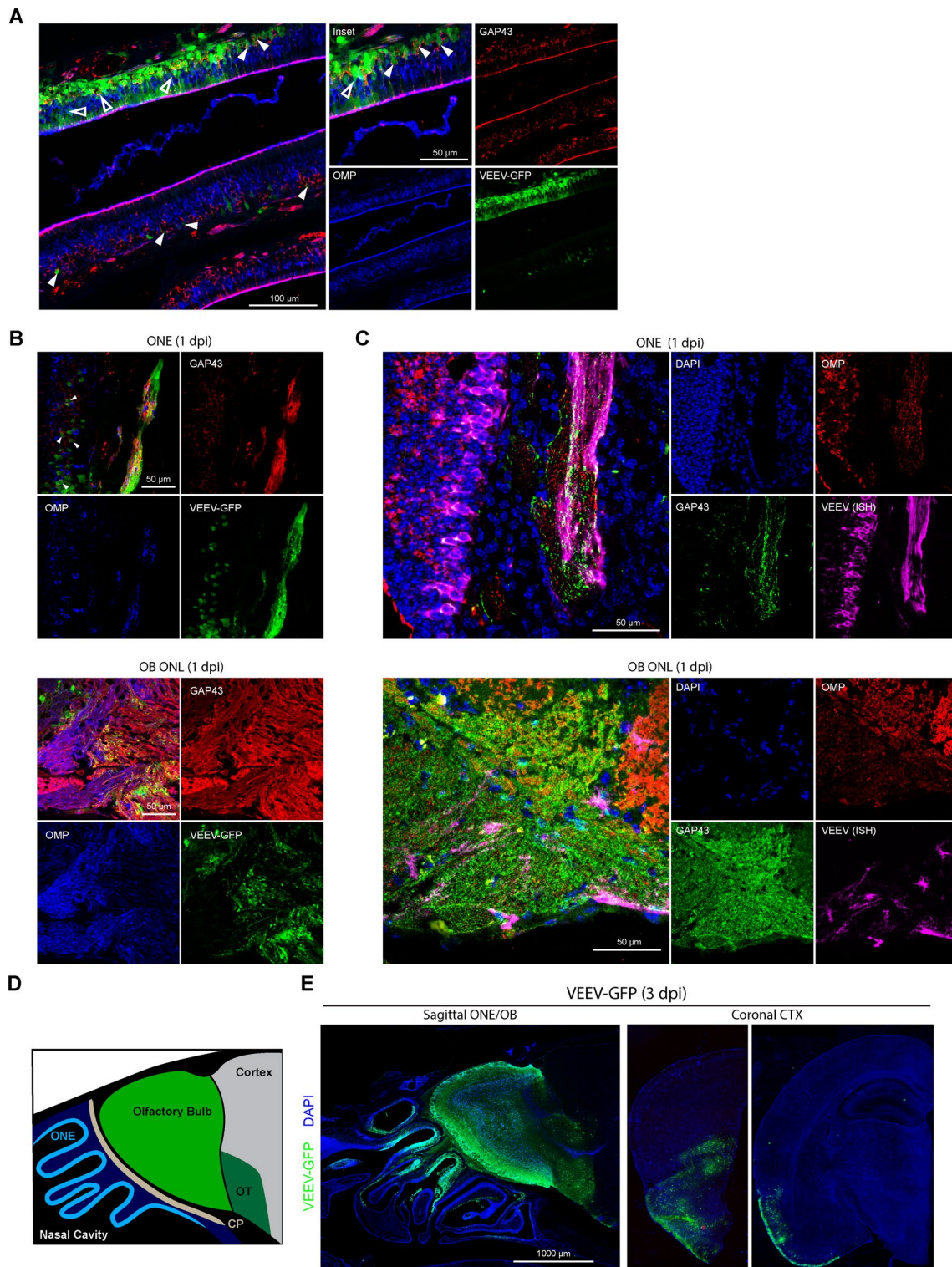


Fig. 1 (See legend on previous page.)

are observed throughout the ONE and OB, including the glomerular, mitral cell, and ganglion cell layers (Fig. 1D, E). At this timepoint, VEEV infection continues to spread into the forebrain along the olfactory tract and piriform CTX (Fig. 1E). Together, these data indicate that VEEV may utilize both immature and mature OSNs for anterograde transport into the OB.

### Higher levels of expression of a VEEV receptor, *Ldlrad3*, underlies enhanced tropism to iOSN

Despite the knowledge that peripheral neurons, including OSNs, are targets for many neurotropic viruses, there are few studies reporting their differential expression of viral entry receptors and innate immune responses [19–21]. To determine whether the SARS-CoV-2 entry receptor angiotensin converting enzyme (ACE2) is an ISG within cells of the ONE, Ziegler et al. performed single-cell RNA sequencing of murine nasal epithelium derived from mice

12 h after i.n. administration of saline versus IFN $\alpha$  ( $10^4$  U) [22]. While they found little to no ACE2 expression in iOSN or mOSN (with or without IFN $\alpha$  exposure), they provided a large data set for investigation of the differential expression of other viral entry receptor mRNAs and overall innate immune response networks in iOSN and mOSN [23]. To define differences between transcriptional signatures of iOSN and mOSN that would underlie the observed enhanced infectivity of VEEV to iOSN, we analyzed differentially expressed genes (DEG) between the two cell types under saline treatment. As expected, the top DEG included genes involved in olfactory sensory perception, cilium development, and ion channel/transport protein expression (*Adcy3*, *Omp*, *Pde1c*, *Cngb1*, *Cnga4* (Additional file 3: Fig. S2A) [24, 25]. Similarly, gene set enrichment analysis (GSEA) using murine gene ontology (GO) pathways identified key differences in pathways associated with neuronal differentiation, axonal

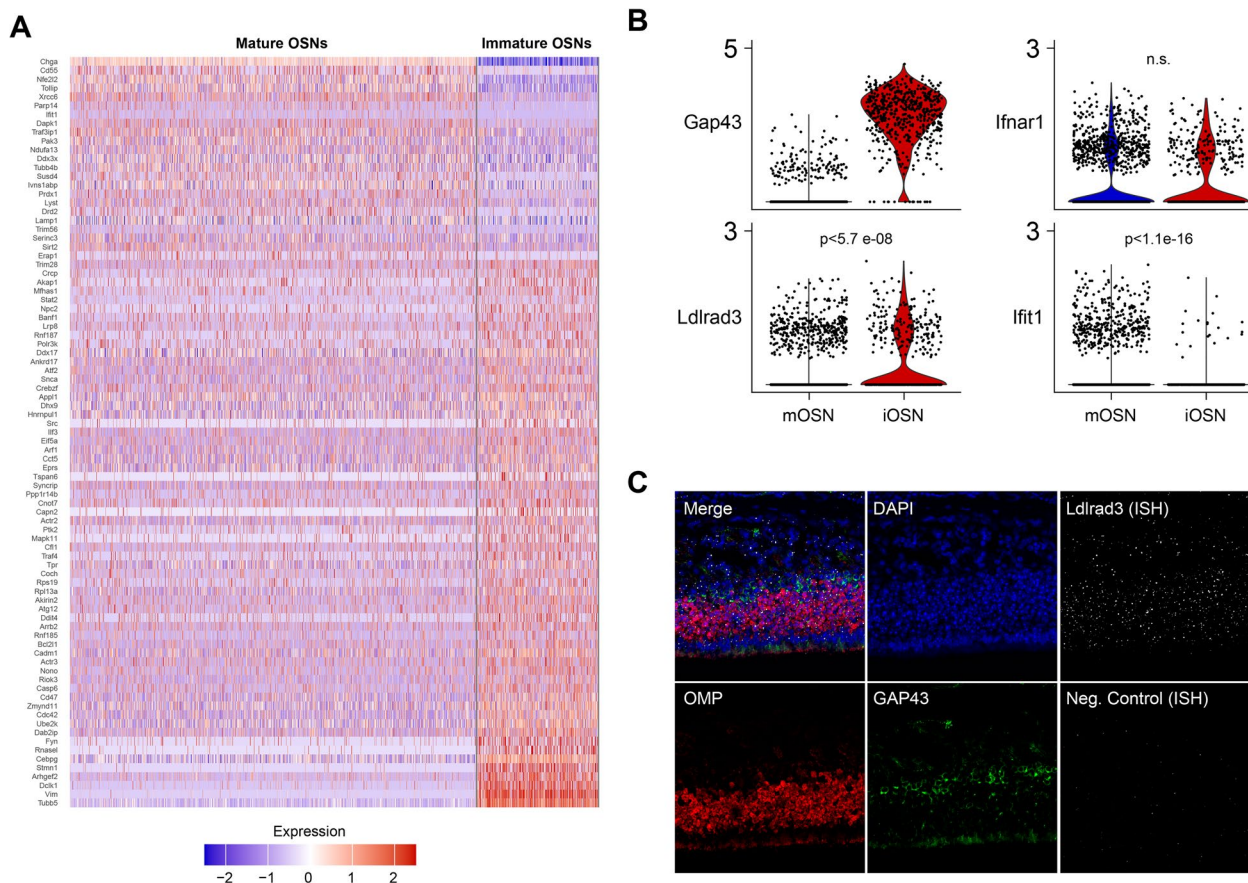


**Fig. 2** Differential expression of innate immune genes and *LDLRAD3* in OSN. **A** Reanalysis of scRNA-seq data set (Ziegler et al., 2020) which captured a large population of both immature and mature murine OSN. Heatmap of DEGs belonging to GO terms (Innate Immune Response, Response to Virus, Response to Type-1 Interferon, Response to Interferon Alpha, and Response to Interferon Beta ( $N = 1816$  mOSN, 539 iOSN from two mice)). **B** Violin plot of expression of candidate genes relevant to VEEV infection and interferon signaling in mature and immature OSN. **C** FISH of *Ldlrad3* (gray) expression in OMP+ (red) and GAP43+ (green) OSNs within the ONE. Images depict representative staining from  $N = 3$  mice.  $P$  values are indicated

**Table 1** GSEA analysis of candidate innate immune GO pathways in mOSN and iOSN

GO pathway	ID	Adj. P Val	NES
Innate immune response	GO:0045087	0.68	1.081
Response to virus	GO:0009615	0.69	1.082
Response to type 1 interferon	GO:0034340	0.99	0.539
Response to interferon alpha	GO:0035455	0.94	-0.683
Response to interferon beta	GO:0035456	0.80	0.99

growth and synapse formation between iOSN and mOSN (Additional file 3: Fig. S2B). While mRNAs of genes relating to innate immunity or control of virus infection were not among the top DEG, some genes associated with GO pathways, including Innate Immune Response, Response to Virus, Response to Type 1 Interferon, Response to Interferon Alpha, and Response to Interferon Beta, were differentially expressed between iOSN and mOSN (Fig. 2A). For example, mRNA levels of Interferon Induced Protein with Tetratricopeptide Repeats 1 (*Ifit1*) was significantly higher in mOSN (Fig. 2B). However, none of these pathways were more significantly enriched by GSEA in either OSN population (Table 1), consistent with lack of differences in mRNA expression levels of IFN $\alpha\beta$  receptor (*Ifnar1*) (Fig. 2B, Additional file 3: Fig. S2B). Together, broad differences in innate immunity do not explain the observed early VEEV tropism and infection of iOSN compared with mOSN. However, mRNA levels of a VEEV receptor, *Ldlrad3* [4], are significantly higher in iOSN versus mOSN (Fig. 2B). While detection of *Ldlrad3* mRNA via fluorescent in situ hybridization (FISH) was observed in both iOSN and mOSN (Fig. 2C), it is likely that overall difference in levels of expression of *Ldlrad3* underlie earlier infection of iOSN.

#### Intranasal IFN $\alpha$ administration induces rapid ISG expression in olfactory sensory neurons

Given that OSN exhibit low levels of expression of innate immune molecules at baseline, we analyzed the scRNAseq data set deposited by Ziegler et al. for DEG in iOSN and mOSN following intranasal IFN $\alpha$  ( $10^4$  U, 12 h) treatment [22, 23]. Both OSN cell types exhibit similar DEG (Fig. 3A, B). As expected DEGs and GSEA indicate strong enrichment of ISGs relating to Type 1 interferon responses following treatment, which was broader for mOSN (Additional file 3: Fig. S2C, D). Overall, this indicates that these cells, critical to early ONE replication and neuroinvasion into the OB, are responsive to such treatment. To validate ISG expression in the ONE and OB in a separate cohort of mice, we examined candidate ISG expression in total nasal cavity (NC) and OB following similar i.n. administration of recombinant

murine IFN $\alpha$  ( $8 \times 10^4$  U) followed by quantitative (q)PCR. Robust upregulation of ISG, including *Ifit1*, *Irf7*, *Ifitm3*, *Isg20*, and *cGas*, was observed in both the nasal cavity and OB at 24 h post-treatment with IFN $\alpha$  compared with vehicle-treated animals (Fig. 3C). To determine if IFN $\alpha$  also altered expression of *Ldlrad3*, we quantified *Ldlrad3* expression as assessed by FISH within the ONE following IFN $\alpha$  treatment at 12 hpi during VEEV infection (Fig. 3D, Additional file 2: Fig. S1C). While *Ldlrad3* expression was enhanced by VEEV infection, IFN $\alpha$  treatment did not synergistically impact its level of expression. Overall, these data indicate that IFN $\alpha$  treatment elicits rapid IFN response in both the ONE and OB, suggesting a potential therapeutic approach for limiting infection and neuroinvasion along this route.

#### VEEV-mediated induction of endogenous IFN and ISGs is delayed within infected olfactory routes

While endogenous IFN signaling is critical for controlling VEEV infection in the periphery [7], the extent to which it controls VEEV infection and dissemination along the olfactory route is unknown. Knowledge of the kinetics of this response is also important for determining if exogenous administration of IFN $\alpha$  would be expected to limit VEEV neuroinvasion. To address this, IFN mRNA expression within the nasal cavity and OB was assessed in uninfected animals and at various timepoints (12, 24, 48 h) post-infection (hpi). IFN $\alpha$  mRNA is not significantly upregulated in the nasal cavity or OB until 48 hpi (Fig. 4A), while IFN $\beta$  mRNA induction is observed at 12 and 24 hpi within the nasal cavity, with significant induction at 24 hpi in the OB (Fig. 4B). Separate analyses of ISG mRNAs linked to inhibition of alphavirus infection showed similarly delayed onset of expression in the nasal cavity and OB (Fig. 4C–H) [26–31]. Only IRF7 was upregulated within 24 hpi (Fig. 4D), with all other candidates not exhibiting expression in both the NC and OB until 48 hpi (Fig. 4C–H). These data indicate potential windows of intervention with i.n. administered IFN $\alpha$  after i.n. exposure to VEEV.

#### Intranasal IFN $\alpha$ treatment early after VEEV exposure delays morbidity and promotes survival

To determine if i.n. administration of IFN $\alpha$  during early VEEV infection would improve outcomes following VEEV infection, IFN $\alpha$  treatment ( $8 \times 10^4$  U) was administered concomitantly or at 1 and 3 h after i.n. VEEV infection (ZPC-738, 10 pfu) of wild-type mice. Pre-treatment (0 hpi) with IFN $\alpha$  delays morbidity, as assessed via encephalitic scoring and weight loss, compared with similarly infected vehicle-treated mice (Fig. 5A). Specifically, weight loss was significantly lower in IFN $\alpha$ -treated mice, and onset lagged approximately 2 days behind that of

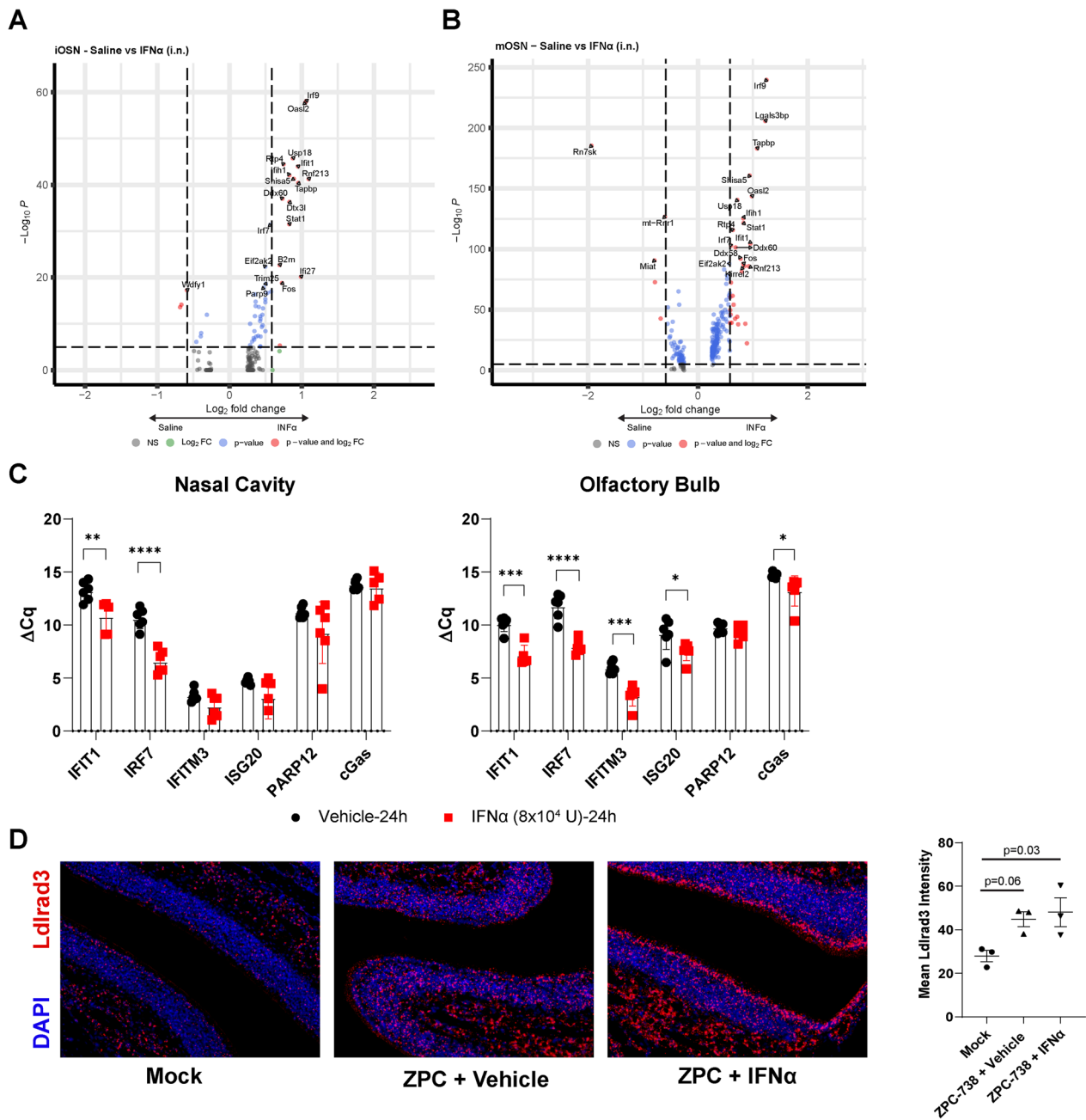


**Fig. 3** Single-dose intranasal IFN $\alpha$  treatment stimulates ISG expression in OSNs and OB. **A** Volcano plot of DEGs within immature OSNs following intranasal saline (negative) or IFN $\alpha$  (positive) treatment ( $1 \times 10^4$  U, 12 h,  $N=539$  saline, 561 IFN $\alpha$  from two mice). **B** Volcano plot of DEGs within mature OSNs following intranasal saline (negative) or IFN $\alpha$  (positive) treatment ( $1 \times 10^4$  U, 12 h,  $N=1816$  saline, 2076 IFN $\alpha$  from two mice). **C** Representative ISG expression within nasal cavity and olfactory bulb homogenates following intranasal IFN $\alpha$  ( $8 \times 10^4$  U, 24 h,  $N=5-6$ ) treatment. **D** FISH of Ldlrad3 expression (red) following vehicle or IFN $\alpha$  co-administration during intranasal VEEV-ZPC (10 pfu, 12 hpi,  $N=3$ ). Error bars indicate mean  $\pm$  SEM.  $\Delta$ Cq were compared via unpaired *t* test. Ldlrad3 expression was compared by one-way ANOVA, followed by Tukey multiple comparison. Statistical values are indicated as follows \* $P < 0.05$ ; \*\* $P < 0.01$ ; \*\*\* $P < 0.001$ ; \*\*\*\* $P < 0.0001$  unless otherwise stated

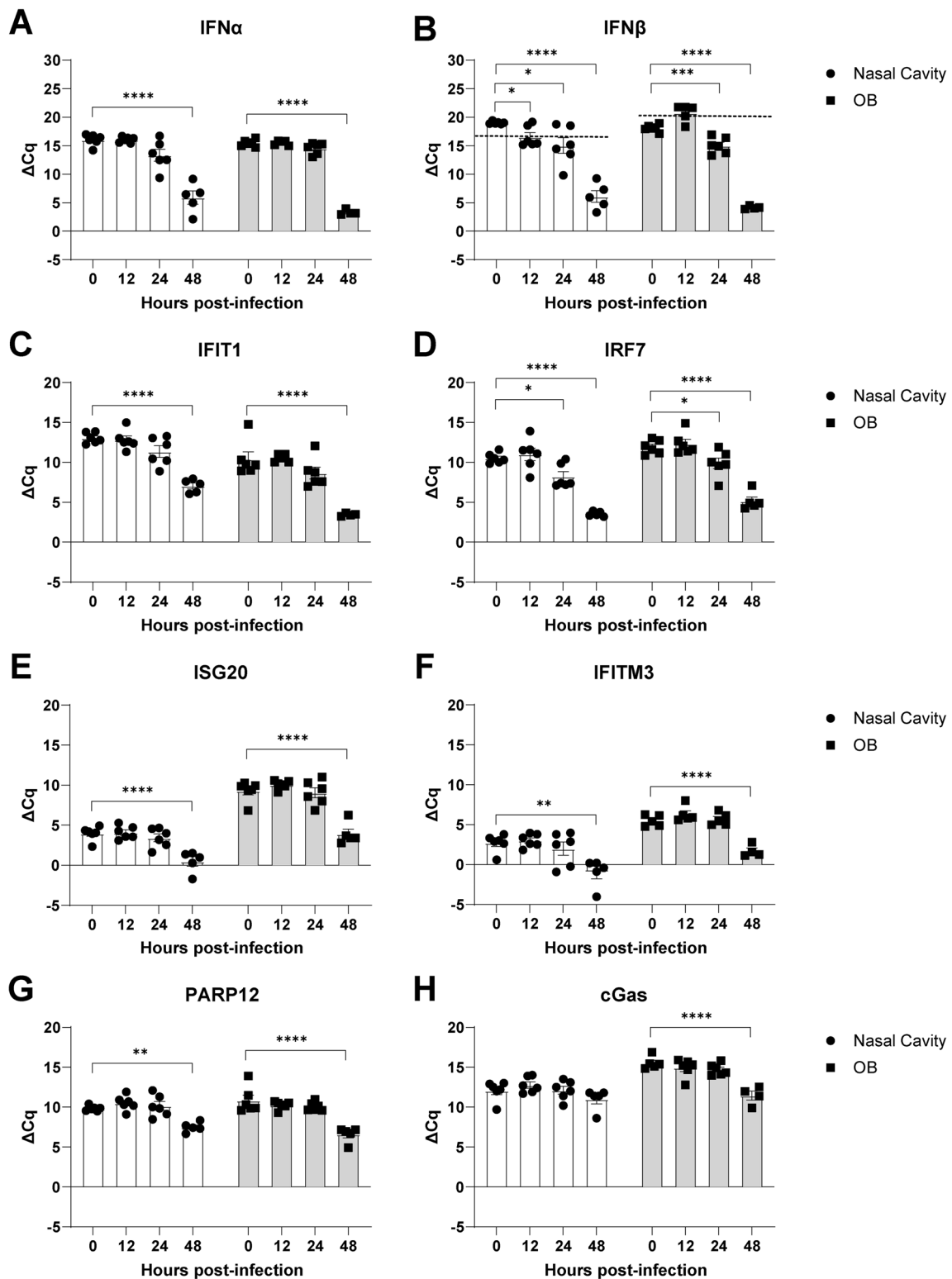


**Fig. 4** Interferon response in nasal cavity and OB is delayed relative to infection. **A, B** Induction of endogenous type-I interferons, IFN $\alpha$  (**A**) and IFN $\beta$  (**B**), expression within nasal cavity and olfactory bulb homogenates following intranasal inoculation of VEEV-ZPC-738 (10 pfu). **C–H** Upregulation of candidate interferon stimulated genes (ISGs) associated with restricting VEEV and/or alphavirus replication induced nasal cavity and olfactory bulb homogenates at various timepoints following intranasal inoculation of VEEV-ZPC-738 (10 pfu). Error bars indicate mean  $\pm$  SEM,  $N=5-6$ .  $\Delta Cq$  were compared via one-way ANOVA, followed by Dunnett's multiple comparison test. Statistical values are indicated as follows \* $P < 0.05$ ; \*\* $P < 0.01$ ; \*\*\* $P < 0.001$ , \*\*\*\* $P < 0.0001$  unless otherwise stated

vehicle-treated VEEV-infected mice (Fig. 5A, left). While VEEV encephalitic signs were similar between vehicle- and IFN $\alpha$ -treated animals, scores were significantly lower and delayed by approximately 2 days in IFN $\alpha$ -treated mice (Fig. 5A, middle, Additional file 4: Fig. S3A). IFN $\alpha$ -treatment at the time of VEEV infection extended mean survival time (+2 dpi MST) but was ultimately insufficient to improve overall mortality (Fig. 5A, right). As knowledge of exposure to VEEV may be delayed, we determined whether post-infectious IFN $\alpha$  treatment at 1 or 3 hpi impacts disease and survival after i.n. infection with VEEV. Both treatment paradigms significantly delayed onset of encephalitic sequelae and weight loss compared with vehicle-treated VEEV-infected mice (Fig. 5B, left and middle, Additional file 4: Fig. S3B). However, weight was not as well-maintained as observed during concomitant IFN $\alpha$  and VEEV i.n. exposure compared with similarly infected vehicle-treated mice, especially when IFN $\alpha$  was administered at 3 hpi. Similar to concomitant treatment, IFN $\alpha$  treatment extended mean survival time (+2 dpi and +1.6 dpi, respectively), without reducing overall mortality (Fig. 5B, right).

To determine if i.n. administration of IFN $\alpha$  limited VEEV replication within the ONE and/or CNS dissemination, viral titers were assessed in IFN $\alpha$ -treated animals. For mice administered IFN $\alpha$  at the time of VEEV infection (0 hpi), viral titers were assessed at 1, 3, and 5 dpi via standard plaque assays. In contrast with vehicle-treated animals, viral titers were undetectable in the brain (OB, CTX) or sera in IFN $\alpha$ -treated mice at 1 dpi (Fig. 5C). By 3 dpi, VEEV was detectable in the majority of CNS tissues derived from vehicle- and IFN $\alpha$ -treated mice (VEEV OB: 5/6; CTX: 4/6). However, overall VEEV titers in OBs and cortices derived from IFN $\alpha$ -treated mice were significantly reduced at this time-point compared with similarly infected vehicle-treated animals (Fig. 5C). IFN $\alpha$  treatment, however, failed to control viremia beyond 1 dpi, as viral titers were equivalent in both treatment groups of VEEV-infected mice

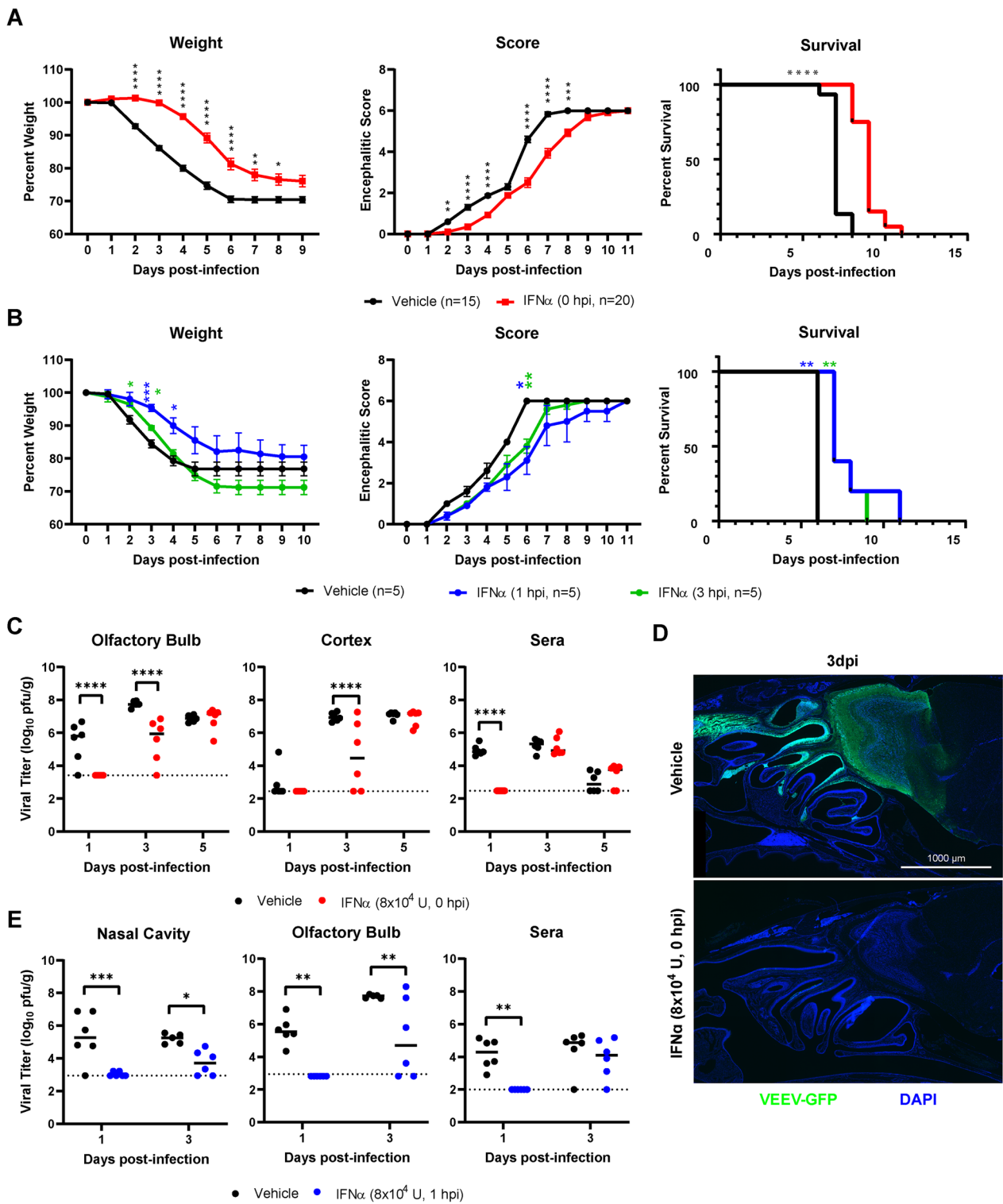
by 3 dpi. Similarly, VEEV viral titers in IFN $\alpha$ -treated mice reached equivalency to vehicle-treated mice by 5 dpi in all CNS regions (Fig. 5C). Direct observation of i.n. ZPC-738-GFP infection (50 pfu) in fixed whole skull mounts revealed strong suppression of infection in the ONE and OB at 3 dpi in IFN $\alpha$ -treated compared to vehicle-treated mice, which displayed robust ZPC-738-GFP throughout the ONE, OB, and olfactory tract (Fig. 5D). When infected cells were observed in IFN $\alpha$ -treated ONE, infected iOSNs were similarly observed earlier than mOSNs, suggesting that IFN $\alpha$  does not alter VEEV tropism beyond the period of suppression.

Endogenous IFN $\alpha$  and IFN $\beta$  expression correlated with the presence of VEEV during the time course of infection in the nasal cavity, OB, and cortices (Additional file 4: Fig. S3C, D). In IFN $\alpha$ -treated mice, endogenous IFN $\alpha$  and IFN $\beta$  expression was not as robustly induced until later in infection, correlating with the early suppression of VEEV in these mice. ISGs *Ifit1* and *IRF7*, which rapidly responded to i.n. IFN $\alpha$  previously, were induced by IFN $\alpha$  treatment in the nasal cavity and OB at 1 dpi, despite reduced endogenous Type I interferon expression (Additional file 4: Fig. S3E, F). Expression was similar, but significantly reduced, compared to vehicle control tissues through 3 dpi, suggesting that the effect of IFN $\alpha$  treatment on ISG expression may have begun to wane to levels that allow for VEEV replication during this period.

Finally, similar to concurrent (0 hpi) administration, i.n. IFN $\alpha$  treatment after infection (1 hpi) suppressed early infection, as VEEV viral titers at 1 dpi within the nasal cavity (NC), OB, and sera were undetectable compared with vehicle-treated mice (Fig. 5E). By 3 dpi, infection in the nasal cavity and OB remained significantly reduced in VEEV-infected mice treated with IFN $\alpha$  compared with vehicle-treated animals but was detectable in a majority of animals (VEEV+NC: 4/6, VEEV+OB: 4/6, VEEV+Sera: 5/6).

(See figure on next page.)

**Fig. 5** Intranasal IFN $\alpha$  delays morbidity and promotes survival during VEEV infection by suppressing onset of nasal and CNS infection. **A** Survival curves, weight loss curves, and encephalitis scores of mice co-administered single-dose intranasal IFN $\alpha$  during ZPC-738 (10 pfu) infection ( $N=15-20$  mice from two independent infections). **B** Survival curves, weight loss curves, and encephalitis scores of mice administered single-dose intranasal IFN $\alpha$  1 or 3 h post-infection with VEEV-ZPC-738 (10 pfu) ( $N=5$ ). **C** Viral titers, as measured by plaque assay, from olfactory bulb, cortex, and sera collected at various DPI from mice co-administered intranasal IFN $\alpha$  during ZPC-738 (10 pfu) infection ( $N=6$ ). **D** Immunostaining of intranasal VEEV-ZPC-GFP infection (50 pfu, 3dpi) of sagittal sectioned nasal cavity and forebrain (representative example for  $N=3$  mice). **E** Viral titers from nasal cavity, olfactory bulb, and sera at various DPI to following intranasal IFN $\alpha$  administered 1 h following ZPC-738 (10 pfu) infection ( $N=5-6$ ). Weight loss, encephalitic sequelae scores, and titers were compared via two-way repeated measure ANOVA, followed by Bonferroni's post hoc test. Survival curves were analyzed by Mantel-Cox test. Statistical values are indicated as follows \* $P < 0.05$ ; \*\* $P < 0.01$ ; \*\*\* $P < 0.001$ , \*\*\*\* $P < 0.0001$  unless otherwise stated



## Discussion

In this study, we tracked the spread of VEEV infection from the ONE to the ONL of the OB, examining viral targets, innate immune responses, and the efficacy of post-exposure treatment with i.n. IFN. We found that GAP43+ iOSN were the first cells infected, followed by OMP+mOSN, which both transport VEEV anterograde into the OB. scRNAseq analysis of OSN identified no broad innate immune deficits associated with iOSN to explain their enhanced infectivity compared to mOSN. However, specific changes in key ISGs, including significantly decreased levels of IFIT1 and/or increased expression of the VEEV receptor LDLRAD3 may underlie VEEV tropism to iOSN. The kinetics of ISG expression after i.n. VEEV revealed a significant delay, with robust upregulation occurring after 24 h. To determine if ISG levels could be rescued by exogenously administered IFN we utilized a model of i.n. IFN $\alpha$  treatment at the time of or post-exposure to VEEV infection. We found that IFN $\alpha$  treatment triggers early ISG expression in OSNs, the nasal cavity, and OB, even when administered as a single post-exposure dose. Consistent with this, IFN $\alpha$  treatment delayed onset of VEEV infection in the nasal cavity and OB, reduced encephalitic sequelae and extended survival. These data demonstrate that exogenous IFN $\alpha$  may be a potential post-exposure intervention for VEEV infection, allowing infected individuals time to obtain additional support or other treatments.

In concordance with our findings, previous studies have demonstrated VEEV infection of OSN; however, these studies did not distinguish tropism between iOSN versus mOSN [32, 33]. Axonal transport of VEEV has also been previously described, with detection of VEEV antigen and virions in olfactory nerve fibers crossing the cribriform plate [33]. Depending on their stage in maturation, iOSNs fully project to OB by ~7 days of differentiation, forming functional synapses in OB glomeruli that participate in limited olfaction [34–36]. As these neurons continue to express markers of immaturity, iOSNs represent not only an early site of VEEV infection within the ONE but also a route of anterograde transport to the OB. As VEEV infection propagates within the ONE, infected OMP+mOSNs likely also contribute to additional VEEV anterograde transport of VEEV to OB but may be less critical to initial neuroinvasion along the olfactory tract.

Examination of genetic signatures of iOSN and mOSN at baseline and after IFN $\alpha$  exposure was performed via interrogation of a previously deposited scRNAseq data set [22, 23]. Type-1 IFN induces expression of ISGs, with only a few mediating the anti-viral activity for a specific pathogen. We found no broad deficits in innate immunity or antiviral gene expression at baseline to explain

enhanced infectivity of iOSN over mOSN, with the exception of *Ifit1*, which was more highly expressed in mOSN. IFIT1 has been shown to limit VEEV replication by restricting translation of VEEV in strains that contain a G3A mutation, such as the TC-83 vaccine strain [27]. However, IFIT1 may be involved in other mechanisms that restrict VEEV replication, since within the same study, *Ifit1*<sup>-/-</sup> mice exhibited shorter MST for both WT ZPC-738 and TC-83 (A3G) mutants. In addition, IFIT1 positively enhances ISG expression independently of viral RNA binding downstream of TLR4 activation in macrophages [37]. It is also possible that OSN differentiation induces other protective effects. Neuronal differentiation was observed to restrict VEEV infection in vitro using the AP7 olfactory-derived neuronal cell line [38]. This effect was cell intrinsic for differentiated cells and correlated with enhanced expression of interferon response factor (IRF)-3 and -7. Thus, additional screening of identified genes might be warranted. Most notably, mRNA expression of the VEEV receptor *Ldlrad3* was enhanced in iOSNs compared to mOSN. The endogenous ligand for LDLRAD3 is unknown, and is proposed to be distinct from other LDL receptor family members [39]. The role of LDLRAD3 in the maturation of iOSN is unknown; however, LDLRAD3 modulates amyloid precursor protein in neurons and promotes activity of E3 ubiquitin ligases, both of which impact neurogenesis [39–42].

Intranasal Type I IFN therapy has been explored for various respiratory viruses, including endemic viruses (rhinovirus and influenza) and recently SARS-CoV2 to modulate the severity of disease [43]. Similarly, Type I IFN treatment has been evaluated in other viruses considered to be potential biological weapons, including other encephalitic alphaviruses and hemorrhagic filoviruses, arenaviruses, phleboviruses [44–51]. However, similar studies evaluating the effectiveness intranasal IFN administration against intranasal/aerosol infection are limited [52, 53]. Our study demonstrates that the nasal cavity, including OSNs, responds rapidly to intranasal administration of IFN with detectable changes of ISG expression within 12 h. The antiviral state initiated following early IFN treatment after VEEV infection leads to suppression VEEV replication in the nasal cavity, preventing early expansion of VEEV infection and escape of VEEV into the blood. Previous studies have shown similar transient protection following intranasal VEEV infection, although these studies utilized prophylactic, multiday treatment and pegylation of IFN $\alpha$  (i.p.) [13]. However, IFN treatment is not able to control VEEV–CNS infection indefinitely. It remains unclear from which reservoir VEEV re-emerges after the effects of exogenous IFN $\alpha$  waned. It is possible that additional peripheral sites did not receive sufficient exogenous IFN $\alpha$  to fully prevent

VEEV infection, allowing for infection of the ONE and OB via hematogenous routes. Alternatively, VEEV may eventually circumvent the induced IFN response within the ONE. This is also consistent with the delayed VEEV expansion in the ONE despite sustained expression of ISGs, such as *Ift1* and *Irf7*, throughout the course of VEEV infection. Encephalitic alphaviruses have evolved immune evasion mechanisms that inhibit host IFN responses and allow virus replication in infected cells. IFN signaling is suppressed by global shut-off of host transcription and translation and inhibition of STAT-1 signaling by capsid and capsid-independent mechanisms [8, 9, 12].

Intranasal delivery has been shown to enhance IFN delivery to rodent and non-human primate brain, especially the OB [14, 15]. Consistent with this model, we observed ISG expression in the OB of treated mice and sustained suppression of OB viral titers in the presence of normal viremia at 3 dpi. This may indicate additional protection of CNS infection downstream of ONE infection. We've reported previously that OB is also an early site of VEEV–CNS infection following subcutaneous infection [3]. Models utilizing subcutaneous or intravenous inoculation could potentially elucidate whether protection of OB is due to local IFN signaling or predominately secondary to delayed replication in the ONE.

Overall, intranasal IFN treatment delays onset of morbidity and extension of survival in a highly lethal animal model of VEEV infection. ZPC-738 is an enzootic strain that is completely lethal in mice. Such a disease course does not reflect the lethality associated with VEEV infection in humans. Approximately, <1% of patients with VEEV succumb to the infection [1, 54]. Therefore, the IFN treatments strategies explored herein may yet be more effective in protecting against lethal VEEV encephalitis in patients. Certainly, early intervention will likely be the most effective, but additional studies evaluating sustained and late IFN $\alpha$  treatment are warranted. Repeated or chronic type I interferon therapy has been associated with side effects of flu-like symptoms, fatigue, weight-loss, and neurological sequelae, including cognitive impairment and depression [55]. These effects have been modeled in animals studies, and would need to be accounted for in repeated-treatment models [56–58]. However, sustained IFN $\alpha$  expressed by adenovirus vector has shown some promise of mitigating encephalitic alphavirus infection independently of high dose, bolus treatments [44, 46]. Alternatively, future studies may continue to leverage murine models to explore IFN modification and delivery strategies. Pegylation of Type I interferon sustains bioavailability, and improved outcomes against VEEV when administered i.p. [13]. Other

modifications focusing on enhancing retention in the nasal cavity with modification or in situ mucoadhesive gel solution may be utilized [59, 60]. However, modifications would need to be evaluated for ease of delivery to the ONE, the effect on IFN delivery to CNS, and how VEEV neuroinvasion would be impacted, especially in those strategies that may disrupt the nose-to-brain barriers [61].

#### Abbreviations

CHIKV	Chikungunya virus
SINV	Sindbis virus
SFV	Semliki Forest virus
RRV	Ross River virus
VEEV, EEEV, WEEV	Venezuelan, Eastern, and Western equine encephalitis viruses
i.n.	Intranasal
OSN	Olfactory sensory neuron
LDLRAD3	Low Density Lipoprotein Receptor Class A Domain Containing 3
IFN	Type I interferons
ISG	Interferon-stimulated genes
OB	Olfactory bulb
CTX	Cortex
ONE	Olfactory neuroepithelium
ONL	Olfactory nerve layer
ACE2	Angiotensin converting enzyme 2
GSEA	Gene set enrichment analysis
GO	Gene ontology
IFIT1	Interferon Induced Protein with Tetratricopeptide Repeats 1
DEG	Differentially expressed genes
scRNAseq	Single cell RNA sequencing
IRF	Interferon response factor

#### Supplementary Information

The online version contains supplementary material available at <https://doi.org/10.1186/s12974-023-02960-1>.

##### Additional file 1: Table S1. qPCR Primers.

**Additional file 1: Fig S1.** Morbidity and survival curves for i.n. VEEV ZPC-738 infection. **A)** Model of intranasal inoculation of VEEV strain, ZPC-738 (10 pfu). Weight curves and encephalitis scores depict immediate and progressive weight loss and progression of morbidity of following infection. Survival curves depict lethality (6–7 DPI) of 8–10 week old C57BL/6J mice following ZPC-738 inoculation intranasal routes. **B)** Representative FISH staining of VEEV genome (magenta) in naive ONE counterstained with OMP + (red) and GAP43 + (green). **C)** Representative FISH staining of *Ldlrad3* expression (red) or negative control probe in naive ONE. Error bars indicate mean  $\pm$  SEM,  $N=8$  from two independent infections.

**Additional file 1: Fig S2.** Differential expression of OSN genes. **A)** Volcano plot of DEGs between mature (negative) and immature (positive) OSNs ( $N=1816$  mOSN, 539 iOSN from two mice). **B)** Top GO terms identified by GSEA analysis between mature (blue) and immature (red) OSNs ordered by normalized enrichment score (NES). **C)** Top GO terms of genes enriched as identified by GSEA analysis in iOSN ( $N=539$  saline, 561 IFN $\alpha$  from two independent mice) and mature OSNs ( $N=1816$  saline, 2076 IFN $\alpha$  from two mice) following intranasal saline (blue) or interferon alpha (red) treatment ( $1 \times 10^4$  U, 12 h). **D)** Heatmap of DEGs belonging to GO terms (Innate Immune Response, Response to Virus, Response to Type-1 Interferon, Response to Interferon Alpha, and Response to Interferon Beta) between saline or IFN $\alpha$  treated mice.

**Additional file 1: Fig S3.** Intranasal IFN $\alpha$  treatment induces similar ISG response over duration VEEV infection despite delayed endogenous

Type-1 interferon expression. **A**) Binned encephalitis scores of mice co-administered single-dose intranasal IFN $\alpha$  during ZPC-738 (10 pfu) infection ( $N=15-20$  mice from two independent infections). **B**) Binned encephalitis scores of mice administered single-dose intranasal IFN $\alpha$  1 or 3 h post-infection with VEEV ZPC-738 (10 pfu) ( $N=5$ ). **C, D**) Induction of endogenous type-1 interferons, IFN $\alpha$  (**C**) and IFN $\beta$  (**D**), expression within nasal cavity, olfactory bulb, and cortex homogenates following intranasal IFN $\alpha$  treatment ( $8 \times 10^4$  U) co-administered during VEEV-ZPC-738 (10 pfu) infection. **E, F**) Representative ISG expression within nasal cavity, olfactory bulb, and cortex homogenates following intranasal IFN $\alpha$  ( $8 \times 10^4$  U, 0 hpi) treatment at multiple timepoints during ZPC-738 (10 pfu) infection ( $N=5-6$ ). Error bars indicate mean  $\pm$  SEM,  $N=8$  from two independent infections.  $\Delta$ Cq were compared via unpaired t-test. Statistical values are indicated as follows \*,  $P < 0.05$ ; \*\*,  $P < 0.01$ ; \*\*\*,  $P < 0.001$ ; \*\*\*\*,  $P < 0.0001$  unless otherwise stated.

### Acknowledgements

We would like to thank Drs. Michael Diamond and Natasha Kafai (Dept. of Medicine, WUSM) for guidance and shared reagents for Ldlrad3 detection, Katie Madden (Dept. of Medicine, WUSM) for assistance in early experiments, Wandy Beatty of the Molecular Microbiology Imaging Facility (WUSM) for advice on confocal imaging. Wei Yang (Department of Genetics) for scRNAseq advice.

### Author contributions

MDC performed VEEV infection experiments in vivo. MDC, NRK, and QW processed tissues for ISG analysis. MDC and XJ performed and analyzed IHC experiments. HS generated stocks of VEEV and assisted with tissue collection. MDC analyzed scRNAseq data. RSK and WBK obtained funding and supervised research. RSK, MJM, WBK, MDC designed the project. RSK and MDC wrote the initial draft of this paper, with all other authors providing comments.

### Funding

Funding for this study was provided by R01AI175524 and R35NS122310 (to RSK).

### Availability of data and materials

The scRNAseq data set analyzed during the current study are available in the Broad Institute repository, [https://singlecell.broadinstitute.org/single\\_cell/study/SCP832?scpr=the-alexandria-project#study-summary](https://singlecell.broadinstitute.org/single_cell/study/SCP832?scpr=the-alexandria-project#study-summary). All other data generated and analyzed during this study are included in the published article and its supplementary information files.

### Declarations

#### Ethics approval and consent to participate

Not applicable.

#### Consent for publication

Not applicable.

#### Competing interests

The authors declare they have no competing interests.

Received: 2 August 2023 Accepted: 14 November 2023

Published online: 17 January 2024

### References

- Salimi H, Cain MD, Klein RS. Encephalitic arboviruses: emergence, clinical presentation, and neuropathogenesis. *Neurotherapeutics*. 2016;13(3):514–34.
- Cain MD, Salimi H, Gong Y, Yang L, Hamilton SL, Heffernan JR, et al. Virus entry and replication in the brain precedes blood-brain barrier disruption during intranasal alphavirus infection. *J Neuroimmunol*. 2017;15(308):118–30.
- Salimi H, Cain MD, Jiang X, Roth RA, Beatty WL, Sun C, et al. Encephalitic alphaviruses exploit caveola-mediated transcytosis at the blood-brain barrier for central nervous system entry. *MBio*. 2020;11(1):e02731–e2819.
- Ma H, Kim AS, Kafai NM, Earnest JT, Shah AP, Case JB, et al. LDLRAD3 is a receptor for Venezuelan equine encephalitis virus. *Nature*. 2020;588(7837):308–14.
- Basore K, Ma H, Kafai NM, Mackin S, Kim AS, Nelson CA, et al. Structure of Venezuelan equine encephalitis virus in complex with the LDLRAD3 receptor. *Nature*. 2021;598(7882):672–6.
- Ma B, Huang C, Ma J, Xiang Y, Zhang X. Structure of Venezuelan equine encephalitis virus with its receptor LDLRAD3. *Nature*. 2021;598(7882):677–81.
- Schoneboom BA, Lee JS, Grieder FB. Early expression of IFN-alpha/beta and iNOS in the brains of Venezuelan equine encephalitis virus-infected mice. *J Interferon Cytokine Res*. 2000;20(2):205–15.
- Bhalla N, Sun C, Lam LKM, Gardner CL, Ryman KD, Klimstra WB. Host translation shutoff mediated by non-structural protein 2 is a critical factor in the antiviral state resistance of Venezuelan Equine Encephalitis Virus. *Virology*. 2016;496:147–65.
- Garmashova N, Atasheva S, Kang W, Weaver SC, Frolova E, Frolov I. Analysis of Venezuelan equine encephalitis virus capsid protein function in the inhibition of cellular transcription. *J Virol*. 2007;81(24):13552–65.
- Garmashova N, Gorchakov R, Volkova E, Paessler S, Frolova E, Frolov I. The old world and new world alphaviruses use different virus-specific proteins for induction of transcriptional shutoff. *J Virol*. 2007;81(5):2472–84.
- Atasheva S, Fish A, Formerod M, Frolova EI. Venezuelan equine encephalitis virus capsid protein forms a tetrameric complex with CRM1 and importin  $\alpha/\beta$  that obstructs nuclear pore complex function. *J Virol*. 2010;84(9):4158–71.
- Simmons JD, White LJ, Morrison TE, Montgomery SA, Whitmore AC, Johnston RE, et al. Venezuelan equine encephalitis virus disrupts STAT1 signaling by distinct mechanisms independent of host shutoff. *J Virol*. 2009;83(20):10571–81.
- Lukaszewski RA, Brooks TJ. Pegylated alpha interferon is an effective treatment for virulent Venezuelan equine encephalitis virus and has profound effects on the host immune response to infection. *J Virol*. 2000;74(11):5006–15.
- Ross TM, Martinez PM, Renner JC, Thorne RG, Hanson LR, Frey WH. Intranasal administration of interferon beta bypasses the blood-brain barrier to target the central nervous system and cervical lymph nodes: a non-invasive treatment strategy for multiple sclerosis. *J Neuroimmunol*. 2004;151(1–2):66–77.
- Thorne RG, Hanson LR, Ross TM, Tung D, Frey WH. Delivery of interferon-beta to the monkey nervous system following intranasal administration. *Neuroscience*. 2008;152(3):785–97.
- Farr BM, Gwaltney JM, Adams KF, Hayden FG. Intranasal interferon-alpha 2 for prevention of natural rhinovirus colds. *Antimicrob Agents Chemother*. 1984;26(1):31–4.
- Sun C, Gardner CL, Watson AM, Ryman KD, Klimstra WB. Stable, high-level expression of reporter proteins from improved alphavirus expression vectors to track replication and dissemination during encephalitic and arthritogenic disease. *J Virol*. 2014;88(4):2035–46.
- Brien JD, Lazear HM, Diamond MS. Propagation, Quantification, Detection, and Storage of West Nile Virus. *Curr Protocols Microbiol*. 2013;31(1):15D.3.1–15D.3.18.
- de Vries L, Harding AT. Mechanisms of neuroinvasion and neuropathogenesis by pathologic flaviviruses. *Viruses*. 2023;15(2):261.
- Steele KE, Twenhafel NA. REVIEW PAPER: pathology of animal models of alphavirus encephalitis. *Vet Pathol*. 2010;47(5):790–805.
- Yang D, Li XJ, Tu DZ, Li XL, Wei B. Advances in viral encephalitis: viral transmission, host immunity, and experimental animal models. *Zool Res*. 2023;44(3):525–42.
- Ziegler CGK, Allon SJ, Nyquist SK, Mbano IM, Miao VN, Tzouanas CN, et al. SARS-CoV-2 receptor ACE2 is an interferon-stimulated gene in human airway epithelial cells and is detected in specific cell subsets across tissues. *Cell*. 2020;181(5):1016–1035.e19.
- Shalek AK, Ordovas-Montanes J. Murine nasal mucosa after intranasal interferon exposure - Single Cell Portal. 2020. [https://singlecell.broadinstitute.org/single\\_cell/study/SCP832/murine-nasal-mucosa-after-intranasal-interferon-exposure#study-summary](https://singlecell.broadinstitute.org/single_cell/study/SCP832/murine-nasal-mucosa-after-intranasal-interferon-exposure#study-summary). Accessed 28 Jun 2023.

24. McClintock TS, Khan N, Xie C, Martens JR. Maturation of the olfactory sensory neuron and its cilia. *Chem Senses*. 2020;45(9):805–22.
25. Boccaccio A, Menini A, Pifferi S. The cyclic AMP signaling pathway in the rodent main olfactory system. *Cell Tissue Res*. 2021;383(1):429–43.
26. Bhalla N, Gardner CL, Downs SN, Dunn M, Sun C, Klimstra WB. Macromolecular synthesis shutoff resistance by myeloid cells is critical to IRF7-dependent systemic interferon alpha/beta induction after alphavirus infection. *J Virol*. 2019;93(24):e00872–e919.
27. Hyde JL, Gardner CL, Kimura T, White JP, Liu G, Trobaugh DW, et al. A viral RNA structural element alters host recognition of nonself RNA. *Science*. 2014;343(6172):783–7.
28. Weiss CM, Trobaugh DW, Sun C, Lucas TM, Diamond MS, Ryman KD, et al. The interferon-induced exonuclease ISG20 exerts antiviral activity through upregulation of type I interferon response proteins. *mSphere*. 2018;3(5):e00209–e218.
29. Poddar S, Hyde JL, Gorman MJ, Farzan M, Diamond MS. The interferon-stimulated gene IFITM3 restricts infection and pathogenesis of arthritogenic and encephalitic alphaviruses. *J Virol*. 2016;90(19):8780–94.
30. Atasheva S, Frolova EI, Frolov I. Interferon-stimulated Poly(ADP-Ribose) polymerases are potent inhibitors of cellular translation and virus replication. *J Virol*. 2014;88(4):2116–30.
31. Schoggins JW, Wilson SJ, Panis M, Murphy MY, Jones CT, Bieniasz P, et al. A diverse array of gene products are effectors of the type I interferon antiviral response. *Nature*. 2011;472(7344):481–5.
32. Charles PC, Walters E, Margolis F, Johnston RE. Mechanism of neuroinvasion of Venezuelan equine encephalitis virus in the mouse. *Virology*. 1995;208(2):662–71.
33. Steele KE, Davis KJ, Stephan K, Kell W, Vogel P, Hart MK. Comparative neurovirulence and tissue tropism of wild-type and attenuated strains of Venezuelan equine encephalitis virus administered by aerosol in C3H/HeN and BALB/c mice. *Vet Pathol*. 1998;35(5):386–97.
34. Cheetham CEJ, Park U, Belluscio L. Rapid and continuous activity-dependent plasticity of olfactory sensory input. *Nat Commun*. 2016;22(7):10729.
35. Liberia T, Martin-Lopez E, Meller SJ, Greer CA. Sequential maturation of olfactory sensory neurons in the mature olfactory epithelium. *eNeuro*. 2019;6(5):ENEURO.0266–19.2019.
36. Huang JS, Kunkhyen T, Rangel AN, Brechbill TR, Gregory JD, Winson-Bushby ED, et al. Immature olfactory sensory neurons provide behaviourally relevant sensory input to the olfactory bulb. *Nat Commun*. 2022;13(1):6194.
37. John SP, Sun J, Carlson RJ, Cao B, Bradfield CJ, Song J, et al. IFIT1 exerts opposing regulatory effects on the inflammatory and interferon gene programs in LPS-activated human macrophages. *Cell Rep*. 2018;25(11):95–106.e6.
38. Schultz KWL, Vernon PS, Griffin DE. Differentiation of neurons restricts Arbovirus replication and increases expression of the alpha isoform of IRF-7. *J Virol*. 2015;89(1):48–60.
39. Ranganathan S, Noyes NC, Migliorini M, Winkles JA, Battey FD, Hyman BT, et al. LRAD3, a novel low-density lipoprotein receptor family member that modulates amyloid precursor protein trafficking. *J Neurosci*. 2011;31(30):10836–46.
40. Noyes NC, Hampton B, Migliorini M, Strickland DK. Regulation of itch and Nedd4 E3 ligase activity and degradation by LRAD3. *Biochemistry*. 2016;55(8):1204–13.
41. Wang S, Bolós M, Clark R, Cullen CL, Southam KA, Foa L, et al. Amyloid  $\beta$  precursor protein regulates neuron survival and maturation in the adult mouse brain. *Mol Cell Neurosci*. 2016;77:21–33.
42. Haouari S, Vourc'h P, Jeanne M, Marouillat S, Veyrat-Durebex C, Lanznaster D, et al. The roles of NEDD4 subfamily of HECT E3 ubiquitin ligases in neurodevelopment and neurodegeneration. *Int J Mol Sci*. 2022;23(7):3882.
43. Padayachee Y, Flicker S, Linton S, Cafferkey J, Kon OM, Johnston SL, et al. Review: the nose as a route for therapy. Part 2 immunotherapy. *Front Allergy*. 2021;2:668781.
44. Wu JQH, Barabé ND, Huang YM, Rayner GA, Christopher ME, Schmaltz FL. Pre- and post-exposure protection against Western equine encephalitis virus after single inoculation with adenovirus vector expressing interferon alpha. *Virology*. 2007;369(1):206–13.
45. Julander JG, Siddharthan V, Blatt LM, Schafer K, Sidwell RW, Morrey JD. Effect of exogenous interferon and an interferon inducer on western equine encephalitis virus disease in a hamster model. *Virology*. 2007;360(2):454–60.
46. O'Brien L, Perkins S, Williams A, Eastaugh L, Phelps A, Wu J, et al. Alpha interferon as an adenovirus-vectored vaccine adjuvant and antiviral in Venezuelan equine encephalitis virus infection. *J Gen Virol*. 2009;90(4):874–82.
47. Jahrling PB, Geisbert TW, Geisbert JB, Swearngen JR, Bray M, Jaax NK, et al. Evaluation of immune globulin and recombinant interferon- $\alpha$ 2b for treatment of experimental ebola virus infections. *J Infect Dis*. 1999;179:S224–34.
48. Smith LM, Hensley LE, Geisbert TW, Johnson J, Stosel A, Honko A, et al. Interferon- $\beta$  therapy prolongs survival in rhesus macaque models of ebola and marburg hemorrhagic fever. *J Infect Dis*. 2013;208(2):310–8.
49. Senthikumar C, Kroeker AL, Smith G, Embury-Hyatt C, Collignon B, Ramirez-Medina E, et al. Treatment with Ad5-porcine interferon- $\alpha$  attenuates ebolavirus disease in pigs. *Pathogens*. 2022;11(4):449.
50. Gowen BB, Barnard DL, Smee DF, Wong MH, Pace AM, Jung KH, et al. Interferon alfacon-1 protects hamsters from lethal pichinde virus infection. *Antimicrob Agents Chemother*. 2005;49(6):2378–86.
51. Gowen B, Ennis J, Bailey K, Vest Z, Scharton D, Sefing E, et al. Single-dose intranasal treatment with DEF201 (adenovirus vectored consensus interferon) prevents lethal disease due to rift valley fever virus challenge. *Viruses*. 2014;1(6):1410–23.
52. Kumaki Y, Ennis J, Rahbar R, Turner JD, Wandersee MK, Smith AJ, et al. Single-dose intranasal administration with mDEF201 (adenovirus vectored mouse interferon- $\alpha$ ) confers protection from mortality in a lethal SARS-CoV BALB/c mouse model. *Antiviral Res*. 2011;89(1):75–82.
53. Smee D, Wong MH, Hurst B, Ennis J, Turner J. Effects of nasal or pulmonary delivered treatments with an adenovirus vectored interferon (mDEF201) on respiratory and systemic infections in mice caused by cowpox and vaccinia viruses. *PLoS ONE*. 2013;9(8): e68685.
54. Kehn-Hall K, Bradfute SB. Understanding host responses to equine encephalitis virus infection: implications for therapeutic development. *Expert Rev Anti Infect Ther*. 2022;20(12):1551–66.
55. Sleijfer S, Bannink M, Van Gool AR, Kruit WHJ, Stoter G. Side effects of interferon- $\alpha$  therapy. *Pharm World Sci*. 2005;27(6):423–31.
56. Reyes-Vázquez C, Prieto-Gómez B, Dafny N. Alpha-interferon suppresses food intake and neuronal activity of the lateral hypothalamus. *Neuropharmacology*. 1994;33(12):1545–52.
57. Blank T, Detje CN, Spieß A, Hagemeyer N, Brendecke SM, Wolfart J, et al. Brain endothelial- and epithelial-specific interferon receptor chain 1 drives virus-induced sickness behavior and cognitive impairment. *Immunity*. 2016;44(4):901–12.
58. Stutte S, Ruf J, Kugler I, Ishikawa-Ankerhold H, Parzefall A, Marconi P, et al. Type I interferon mediated induction of somatostatin leads to suppression of ghrelin and appetite thereby promoting viral immunity in mice. *Brain Behav Immun*. 2021;1(95):429–43.
59. Hauptstein N, Meinel L, Lühmann T. Bioconjugation strategies and clinical implications of Interferon-bioconjugates. *Eur J Pharm Biopharm*. 2022;172:157–67.
60. Agrawal M, Saraf S, Saraf S, Dubey SK, Puri A, Gupta U, et al. Stimuli-responsive In situ gelling system for nose-to-brain drug delivery. *J Control Release*. 2020;10(327):235–65.
61. Ghadiri M, Young PM, Traini D. Strategies to enhance drug absorption via nasal and pulmonary routes. *Pharmaceutics*. 2019;11(3):113.

## Publisher's Note

Springer Nature remains neutral with regard to jurisdictional claims in published maps and institutional affiliations.